

Low coercivity microwave ceramics based on LiZnMn ferrite synthesized via glycine-nitrate combustion

K. D. Martinson^{1,2}, S. S. Kozyritskaya¹, I. B. Panteleev¹, V. I. Popkov^{1,2,3}

¹Saint Petersburg State Institute of Technology (Technical University), Moskovskiy pr. 26, Saint Petersburg, 190013, Russia

²Ioffe Institute, Politechnicheskaya 26, Saint Petersburg, 194021, Russia

³Saint Petersburg University, 26 Universitetskii prospect, Saint Petersburg, 198504, Russia

martinsonkirill@mail.ru

DOI 10.17586/2220-8054-2019-10-3-313-317

Soft magnetic LiZnMn ferrite with low coercivity obtained via glycine-nitrate combustion was estimated in this work. According to SEM, the synthesized ceramics have a grain size ranging from 1.5 to 8 μm and the EDX, AAS and XRD data show that the obtained samples correspond to $\text{Li}_{0.45}\text{Zn}_{0.05}\text{Mn}_{0.06}\text{Fe}_{2.43}\text{O}_4$ structure. The hysteresis loops of LiZnMn ferrite ceramics provide evidence for the magnetically soft nature of the obtained materials. Basic magnetic characteristics, including remanent magnetization, saturation magnetization, and coercive force was also described. For a sample sintered at 1000 °C, the values of saturation magnetization ($4\pi M_s$), residual magnetization (B_r) and coercive force (H_c) were 2644 G, 2139 G and 6.4 Oe, respectively, whereas the sample obtained at 1070 °C shows large values of saturation magnetization (3240 G) and residual magnetization (2459 G) and the coercive force is approximately half (3.4 Oe). Analysis of the influence of thermal treatment provided the possibility to determine necessary conditions for obtaining microwave ceramics based on LiZnMn ferrite via solution combustion method. Grain size distribution was examined to determine their influence on the properties of obtained ceramics.

Keywords: microwave ceramics, spinel ferrites, solution combustion synthesis, soft magnetics.

Received: 18 June 2019

Revised: 20 June 2019

1. Introduction

During the last few decades, the rapid development of microwave technologies has aroused an increased interest in classical high-frequency materials and imposed a new requirement on their electromagnetic parameters [1–3]. Some LiZnMn ferrites have been widely used in microwave devices due to their low coercive forces (H_c), high remanent and saturation magnetizations (M_r and M_s), great mechanical and chemical stabilities, rectangular hysteresis loop, etc. [4–7]. The electromagnetic properties of LiZnMn ferrites depend on factors such as the type of synthesis, degree of crystallinity, particle and grains size, degree of homogeneity for particle and grain sizes [8, 9]. There are many techniques to obtain lithium ferrites, for example, microwave sintering which is the most popular at the moment but has some significant flaws such as long synthesis time, the large grain size of the resulting product and high heterogeneity degree of their size, which negatively affects the final electromagnetic parameters of ceramics [10–13]. One of the more promising methods for obtaining ferrites, which allows improving the above parameters, is the solution combustion method. This method can result in the synthesis of ferrites with small particle and grain sizes, high density and conversion degree, excellent electromagnetic parameters and uniform microstructure [14–19].

In this work, the glycine-nitrate combustion process has been used for preparing initial LiZnMn ferrite powder using glycine as chelating reagent with ratio $G/N = 1.5$ (where G is the glycine mole fraction and N is the nitrate mole fraction). There is the relatively large number of different chelating reagents, such as some organic acids, hydrazine, urea, and others but using the glycine can reduce the amount of residual organic compounds in the final product due to its lower molecular weight than other chelating agents have [20–22]. The received product of glycine-nitrate combustion was heat sintered at various temperatures (1000 and 1070 °C) as a result; microwave ceramics with low coercivity force were obtained.

2. Experimental

This work is devoted to the investigation of microwave ceramics based on the $\text{Li}_{0.45}\text{Zn}_{0.05}\text{Mn}_{0.06}\text{Fe}_{2.43}\text{O}_4$ obtained via glycine-nitrate combustion method. The synthesis was performed under conditions of deficit of the chelating agent ($G/N = 1.5$) in the reaction mixture. Initial lithium, zinc, manganese, and iron crystalline nitrates were dissolved in 100 ml of deionized water and 10 ml of 3M HNO_3 with constant stirring for 2 hours and temperature of 50 °C. Then glycine was added to the reaction solution in an amount exceeding the stoichiometric ratio of 1.5. The solution prepared this way was heated to its autoignition point. During the autoignition process, the brown powder was obtained which was mechanically ground in an agate mortar. The final product was thermally treated at a temperature of 500 °C for 3 hours.

The obtained powder was mechanically processed in a vibration mill (ball diameter = 2 cm) for 2 hours with the addition of bismuth oxide ($\text{LiZnMn}:\text{Bi}_2\text{O}_3$ to 95:5 wt. %) and polyethylene glycol as a binder. The addition of bismuth oxide reduces the sintering temperature, however, despite the fact that its effect on the sintering of lithium ferrites is well studied for solid-phase methods [4], due to the significantly smaller particle size of the original powder and, as a result, a higher specific surface area, the amount of bismuth oxide required to successfully lower the temperature is much higher. Sintering ceramics was carried out at two temperatures (1000 and 1070 °C). The two selected sintering temperatures are most common when lithium-zinc-manganese sintering a ferrite of the similar composition [8, 23].

Qualitative X-ray phase analysis and crystal structure refinement was performed using Rigaku SmartLab 3 powder diffractometer. The average crystallite size (coherent scattering area) was calculated from X-ray diffraction lines broadening using the Scherrer equation:

$$D = \frac{k \cdot \lambda}{\beta \cdot \cos \theta},$$

where k is the crystal shape factor (assumed to be 0.94 in the isometric approximation), λ is the X-ray emission wavelength (CuK_α , $\lambda = 0.15406$ nm), β is the diffraction maximum broadening (in radians), θ is the diffraction peak position (Bragg angle).

The chemical composition and morphology were determined using a TescanVega 3 SBN scanning microscope equipped with an Oxford INCA x -act x -ray spectral microanalysis device and atomic absorption spectrometer AA-7000. The measurement of the magnetic properties was conducted on the vibrating magnetometer Lake Shore 7400. The magnetic characteristics according to the hysteresis loop data were calculated using the vibration method built in the magnetometer's software on vibration magnetometer Lake Shore 7410. Dynamic light scattering and SEM microphotographs were used to determine the average grain size of LiZnMn ceramics obtained at different temperatures. The measurements were carried out using a Shimadzu SALD-7500 nano.

3. Results and discussion

The phase composition of the obtained $\text{Li}_{0.45}\text{Zn}_{0.05}\text{Mn}_{0.06}\text{Fe}_{2.43}\text{O}_4$ powder and ceramics were determined by X-ray powder diffractometry. The obtained data show that initial ferrite powder consists of single-phase lithium-zinc-manganese ferrite (JCPDS card # 52-0278) with an average crystallite size of 25 ± 3 nm (Fig. 1). The conversion degree of synthesized powder was determined to be 95% using an internal standard (α -Si).

Diffractograms of the lithium-zinc-manganese ferrite sintered at 1000 and 1070 °C also show the absence of extraneous phases. The high intensity of the peaks indicates that the obtained ceramics have a high conversion. However, the peak intensities of the obtained sample at 1070 °C are higher than those for the sample sintered at 1000 °C, which indicates a more complete degree of sintering.

The elemental composition and morphology of the obtained lithium-zinc-manganese ferrite were determined by X-ray microanalysis, atomic absorption spectroscopy, and scanning electron microscopy. According to elemental analysis data, the obtained ferrite corresponds to the composition of $\text{Li}_{0.45}\text{Zn}_{0.05}\text{Mn}_{0.06}\text{Fe}_{2.43}\text{O}_4$. Fig. 2 shows the results of SEM for the LiZnMn ferrite ceramics samples sintered at 1000 and 1070 °C. The obtained data suggest that ceramics with grain size from 0.5–10 μm are obtained at both temperatures. In the case of a sample sintered at a temperature of 1000 °C, porous ceramics are observed with an average grain size of 0.5–4.5 μm . The presence of a large number of voids and the appearance of the grains is most likely due to the fact that the lithium-zinc-manganese ferrite ceramics is not completely sintered at a given temperature. In the case of a sample that was sintered at a temperature of 1070 °C the sintering passed completely, which indirectly confirms the XRD data. However, there is an increase in grain size, which ranges from 2–10 μm .

The grain size distribution was determined by a dynamic light scattering method (Fig. 3c and Fig. 3d) and by the analysis of the micrographs in the OriginPro software package (Fig. 3a and Fig. 3b). The obtained data correlate well with each other and indicate that the average crystallite size ranges from 0.5–10 μm . In the case of results obtained

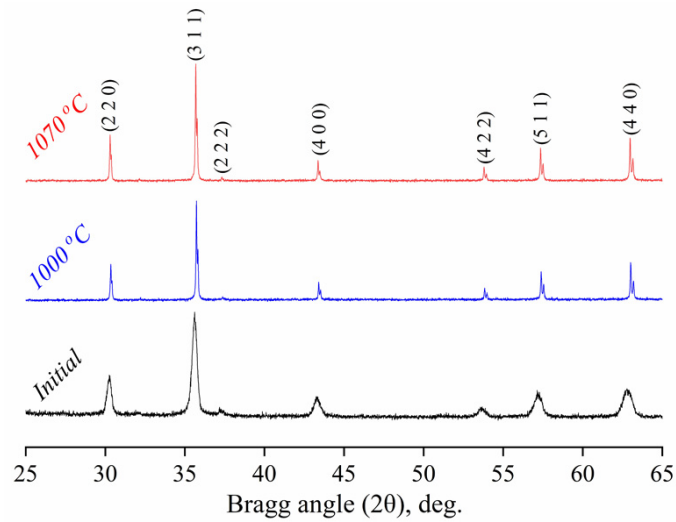


FIG. 1. X-ray diffraction patterns of $\text{Li}_{0.45}\text{Zn}_{0.05}\text{Mn}_{0.06}\text{Fe}_{2.43}\text{O}_4$ initial powder and ceramics

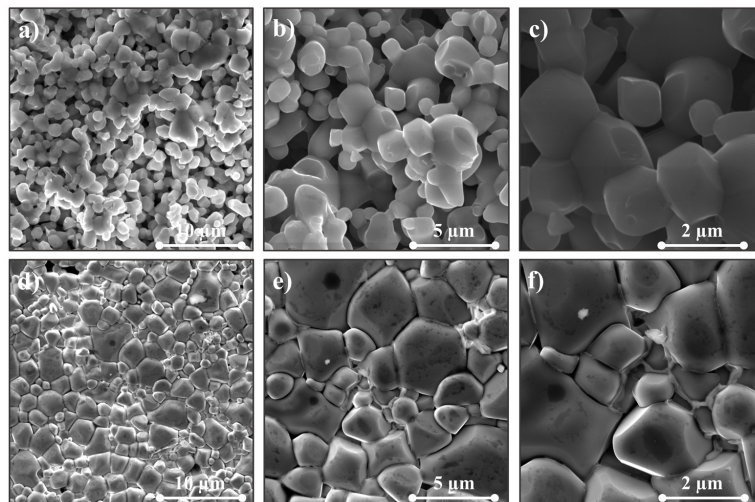


FIG. 2. SEM results of the LiZnMn ferrite ceramics sintered at 1000 and 1070 °C

by the method of dynamic light scattering, the distribution is shifted to the right side in relation to the results of micrographs analysis, which is associated with an insufficient degree of separation of one grain from another.

Figure 4 shows the saturated B–H hysteresis loops at 298 K for lithium-zinc-manganese samples sintered 1000 and 1070 °C. The obtained data indicate that the hysteresis loop of the sample sintered at 1070 °C degrees is approximately half that of the loop for the sample obtained at 1000 °C.

The data in Fig. 5 demonstrate that the saturation magnetization, residual magnetization, and coercive force depended on the sintering temperature.

The saturation magnetization is 2644 G and 3240 G for samples obtained at 1000 and 1070 °C, respectively. Residual magnetization is also higher for a sample sintered at a temperature of 1070 °C (2139 G vs 2458 G). However, the coercive force for a sample sintered at 1000 °C (6.4 Oe) is rough twice the size of the value obtained for a sample sintered at 1070 °C (3.4 Oe). These differences in the magnetic parameters of the obtained ceramic samples are related to both the grain size and to the incomplete degree of sintering of the sample obtained at 1000 °C.

4. Conclusions

The present paper shows the possibility of producing a soft-magnetic low coercivity lithium-zinc-manganese ceramics based on ferrite powder obtained via glycine-nitrate combustion method. The obtained powder and ceramics are chemically and phase-pure and does not contain non-magnetic phases. The low coercivity force (6.4 and 3.4 Oe),

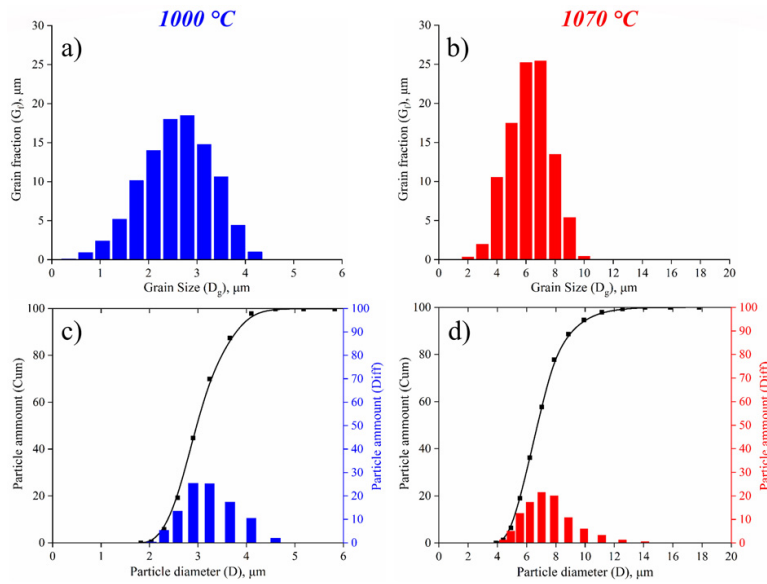


FIG. 3. The grain size distribution of the obtained samples of $\text{Li}_{0.45}\text{Zn}_{0.05}\text{Mn}_{0.06}\text{Fe}_{2.43}\text{O}_4$ ceramics sintered at temperatures of 1000 and 1070 °C

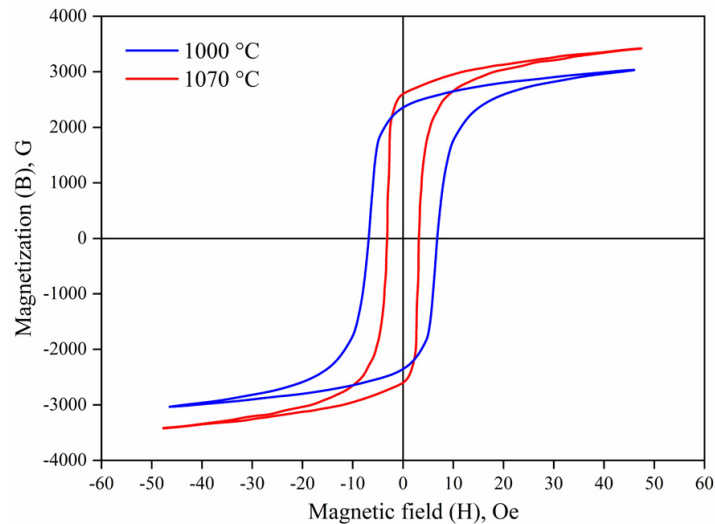


FIG. 4. B-H hysteresis loops of LiZnMn ceramics samples at 298 K

saturation magnetization (3240 and 2644 G) and residual magnetization (2459 and 2139 G) are at the same level as commercial high-frequency ceramics. It is shown that the sintering temperature strongly influences the magnetic characteristics of the obtained ceramics and allows a two-fold reduction in their coercive force.

References

- [1] Asilqbal M., Islam M.U., Ali I., et. al. Study of physical, magnetic and electrical properties of rare-earth substituted Li-Mg ferrites. *Journal of alloys and compounds*, 2017, **692**, P. 322–331.
- [2] Lin Y., Don J.g, Dai J., et. al. Facile synthesis of flowerlike LiFe_5O_8 microspheres for electrochemical supercapacitors. *Inorganic chemistry*, 2017, **56**, P. 14960–14967.
- [3] Abdel-Ghany A.E., Mauger A., Groult H., et. al. Structural properties and electrochemistry of $\alpha\text{-LiFeO}_2$. *Journal of Power Sources*, 2012, **197**, P. 285–291.
- [4] Guo R., Yu Z., Jiang X., et. al. Dispersion spectra of permeability and Permittivity for LiZnMn ferrite doped with Bi_2O_3 . *IEEE Transactions of magnetics*, 2013, **49**, P. 4295–4298.
- [5] Guo R., Yu Z., Yand Y., et. al. Effects of Bi_2O_3 on FMR linewidth and microwave dielectric properties of LiZnMn ferrite. *Journal of Alloys and Compounds*, 2014, **589**, P. 1–4.

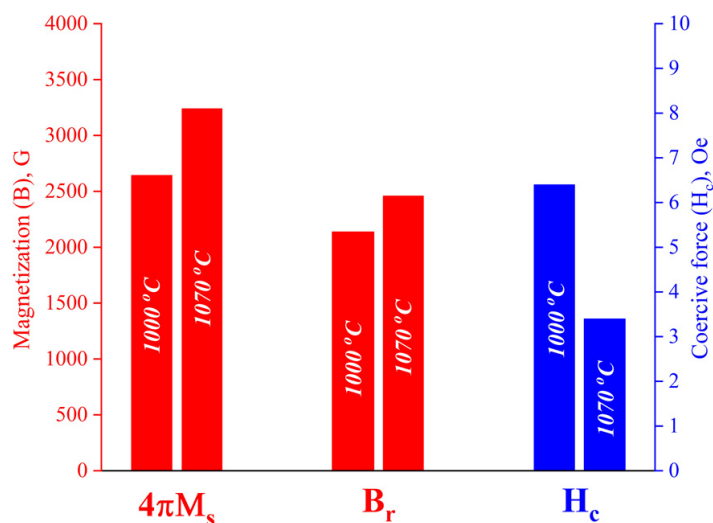


FIG. 5. Saturation magnetization, residual magnetization and coercive force of LiZnMn ceramics

- [6] Silakate S., Wannagon A., Nuntiya A. Influence of ferric oxide on the crystallization of Li-Zn ferrite anorthite and hematite phases at low-temperature ceramic glaze. *Journal of European Ceramic Society*, 2015, **35**, P. 2183–2188.
- [7] Kumar P., Juneja J.K., Prakash C., et. al. High DC resistivity in microwave sintered $\text{Li}_{0.49}\text{Zn}_{0.02}\text{Mn}_{0.06}\text{Fe}_{2.43}\text{O}_4$ ferrites. *Ceramics International*, 2014, **40**, P. 2501–2504.
- [8] Sanatombi S., Sumitra S., Ibetombi S. Influence of sintering on the structural, electrical and magnetic properties of Li-Ni-Mn-Zn ferrite synthesized by citrate precursor method. *Iranian Journal of Science and Technology*, 2018, **42**, P. 2397–2406.
- [9] Teo M.L.S., Kong L.B., Li Z.W., et. al. Development of magneto-dielectric materials based on Li-ferrite ceramics. Densification behavior and microstructural development. *Journal of Alloys and Compounds*, 2008, **459**, P. 557–566.
- [10] Dai Y.M., Wang Y.F., Chen C.C. Synthesis and characterization of magnetic LiFe_5O_8 - LiFeO_2 as a solid basic catalyst for biodiesel production. *Catalysis Communications*, 2018, **106**, P. 20–24.
- [11] Wu H., Li H., Sun G., et. al. Synthesis, characterization and electromagnetic performance of nanocomposites of graphene with α - LiFeO_2 and β - LiFe_5O_8 . *Journal of Materials Chemistry*, 2015, **21**, P. 1–11.
- [12] Srivastava M., Layek S., Singh J., et. al. Synthesis, magnetic and mössbauer spectroscopic studies of Cr doped lithium ferrite nanoparticles. *Journal of Alloys and Compounds*, 2014, **591**, P. 174–180.
- [13] Sohn R.S., Macedo A.A.M., Costa M.M., et. al. Studies of the structural and electrical properties of lithium ferrite (LiFe_5O_8). *Physica Scripta*, 2010, **82**, P. 1–6.
- [14] Martinson K.D., Kondrashkova I.S., Popkov V.I. Synthesis of EuFeO_3 nanocrystals by glycine-nitrate combustion method. *Russian Journal of Applied Chemistry*, 2017, **90**, P. 1214–1218.
- [15] Bachina A., Ivanov V.A., Popkov V.I. Peculiarities of LaFeO_3 nanocrystals formation via glycine-nitrate combustion. *Nanosystems: Physics, Chemistry, Mathematics*, 2017, **8**, P. 647–653.
- [16] Rubalajyothi P., Nehru L.C. Photoluminescence characterization of nanocrystalline $\text{Ba}_{0.97}\text{Ca}_{0.03}\text{SO}_4$:Eu by combustion method. *Nanosystems: Physics, Chemistry, Mathematics*, 2015, **3**, P. 561–565.
- [17] Martinson K.D., Cherepkova I.A., Sokolov V.V. Formation of cobalt ferrite nanoparticles via glycine-nitrate combustion and their magnetic properties. *Glass Physics and Chemistry*, 2018, **44**, P. 21–25.
- [18] Kondrashkova I.S., Martinson K.D., Zakharova N.V., Popkov V.I. Synthesis of nanocrystalline HoFeO_3 photocatalyst via heat treatment of products of glycine-nitrate combustion. *Russian Journal of General Chemistry*, 2018, **88**, P. 2465–2471.
- [19] Popkov V.I., Almjasheva O.V., Nevedomskiy V.N., et. al. Crystallization behavior and morphology of YFeO_3 nanocrystallites obtained by glycine-nitrate combustion. *Nanosystems: Physics, Chemistry, Mathematics*, 2015, **6**, P. 866–874.
- [20] Zhang D., McCartney D.G. Quantitatively evaluating the effect of oxygen/fuel ratio on Fe^{2+} content in HVOF-Sprayed Ni-Zn ferrite coatings. *ASM International*, 2009, **18**, P. 343–352.
- [21] Popkov, Almjasheva O.V. Yttrium Orthoferrite YFeO_3 Nanopowders Formation under Glycine-Nitrate Combustion Conditions. *Russian Journal of Applied Chemistry*, 2014, **87**, P. 167–171.
- [22] Dyachenko S.V., Martinson K.D., Cherepkova I.A., Zhernovoi A.I. Particle size, morphology, and properties of transition metal ferrosinels of the MFe_2O_4 ($\text{M} = \text{Co}, \text{Ni}, \text{Zn}$) type, produced by glycine-nitrate combustion. *Russian Journal of Applied Chemistry*, 2016, **89**, P. 535–539.
- [23] Zhao T., Qin Y., Zhang P., et. al. High-performance, reaction sintered lithium disilicate glass-ceramics. *Ceramics International*, 2014, **40**, P. 12449–12457.